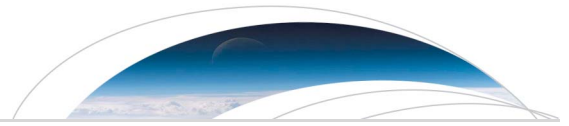




Originally published as:

McPhillips, D., Hoke, G. D., Liu-Zeng, J., Bierman, P. R., Rood, D. H., Niedermann, S. (2016): Dating the incision of the Yangtze River gorge at the First Bend using three-nuclide burial ages. - *Geophysical Research Letters*, 43, 1, pp. 101–110.

DOI: <http://doi.org/10.1002/2015GL066780>



RESEARCH LETTER

10.1002/2015GL066780

Key Points:

- Cosmogenic nuclides ^{10}Be , ^{26}Al , and ^{21}Ne reveal sediment burial ages
- Burial ages indicate an average gorge incision rate of 0.1 to 0.3 km/Myr between 18 and 9 Ma
- Incision slowed by about an order of magnitude after 9 Ma

Supporting Information:

- Texts S1–S4 and Figures S1–S8
- Tables S1–S6

Correspondence to:

D. McPhillips,
devin.mcphillips@gmail.com

Citation:

McPhillips, D., G. D. Hoke, J. Liu-Zeng, P. R. Bierman, D. H. Rood, and S. Niedermann (2016), Dating the incision of the Yangtze River gorge at the First Bend using three-nuclide burial ages, *Geophys. Res. Lett.*, *43*, 101–110, doi:10.1002/2015GL066780.

Received 28 OCT 2015

Accepted 9 DEC 2015

Accepted article online 17 DEC 2015

Published online 6 JAN 2016

Dating the incision of the Yangtze River gorge at the First Bend using three-nuclide burial ages

Devin McPhillips¹, Gregory D. Hoke¹, Jing Liu-Zeng², Paul R. Bierman³, Dylan H. Rood^{4,5}, and Samuel Niedermann⁶

¹Department of Earth Sciences, Syracuse University, Syracuse, New York, USA, ²State Key Laboratory of Earthquake Dynamics, Institute of Geology, China Earthquake Administration, Beijing, China, ³Department of Geology, University of Vermont, Burlington, New York, USA, ⁴Department of Earth Science and Engineering, South Kensington Campus, Imperial College London, London, UK, ⁵Scottish Universities Environmental Research Centre, East Kilbride, UK, ⁶GFZ German Research Center for Geosciences, Potsdam, Germany

Abstract Incision of the Yangtze River gorge is widely interpreted as evidence for lower crustal flow beneath the southeast margin of the Tibetan Plateau. Previous work focused on the onset of incision, but the duration of incision remains unknown. Here we present cosmogenic nuclide burial ages of sediments collected from caves on the walls of the gorge that show the gorge was incised ~1 km sometime between 18 and 9 Ma. Thereafter, incision slowed substantially. We resolve middle Miocene burial ages by using three nuclides and accounting for in situ muogenic production. This approach explains the absolute concentrations of ^{10}Be , ^{26}Al , and ^{21}Ne , as well as $^{26}\text{Al}/^{10}\text{Be}$ and $^{21}\text{Ne}/^{10}\text{Be}$ ratios. A declining incision rate challenges existing geodynamic interpretations by suggesting that either (1) surface uplift has ceased immediately south of the plateau margin or (2) gorge incision is not a useful proxy for the timing of surface uplift.

1. Introduction

On the southeast margin of the Tibetan Plateau, the incision dynamics of the Yangtze River and its major tributaries have become important evidence for inferring the geodynamics of this orogenic plateau. Validity of the hypothesis that lower crustal flow drove crustal thickening, and therefore southeastward expansion of the Tibetan Plateau, depends upon the timing of the onset and propagation of surface uplift [Royden *et al.*, 1997; Clark and Royden, 2000; Clark *et al.*, 2005a, 2005b; Schoenbohm *et al.*, 2006; Cook and Royden, 2008; Royden *et al.*, 2008]. River incision is frequently interpreted as a proxy for surface uplift in the absence of extensive structural evidence for crustal thickening in this region [Wang *et al.*, 1998; Clark *et al.*, 2005b; Schoenbohm *et al.*, 2006; Ouimet *et al.*, 2010]. The major alternative to lower crustal flow is tectonic block extrusion [Tapponnier *et al.*, 1981; Tapponnier, 2001]. This hypothesis attributes crustal thickening and surface uplift on the margin of the plateau to lateral motions along extant strike-slip structures. Recent work has invoked the timing of river incision in its support [Tian *et al.*, 2014].

Despite its importance for deciphering the mechanisms of plateau growth, the history of Yangtze River incision is both controversial and incomplete [Liu-Zeng *et al.*, 2008]. For example, the integration of the modern river network may have occurred before 23 Ma or as late as 1.7 Ma [Clift, 2006; Kong *et al.*, 2009, 2012; Yan *et al.*, 2012]. In addition, previous work has focused on the onset of river incision and given less attention to rates of downcutting after incision began [Clark *et al.*, 2005b; Ouimet *et al.*, 2010; Wang *et al.*, 2012]. This focus partly reflects the limitations of tools such as low-temperature thermochronology, which has limited capacity to resolve post-Miocene incision and cooling, even using state-of-the-art methods [e.g., Herman *et al.*, 2014]. However, recent modeling suggests that surface uplift driven by lower crustal flow will occur over a limited time interval, with a discrete onset and conclusion [see Cook and Royden, 2008, Figure 7]. With this dynamic prediction in mind, we investigate the entire history of Yangtze River incision at its First Bend, on the southeast margin of the Tibetan Plateau (Figure 1).

The First Bend is a hairpin turn entrenched in a 1.5 km deep gorge. This dramatic feature likely marks a major episode of river capture, when the lower and middle Yangtze River diverted the present upper Yangtze away from an ancient river system that drained from the Tibetan Plateau to the South China Sea [Lee, 1934; Barbour, 1936; Clark *et al.*, 2004]. In order to quantify gorge incision through time, we measured terrestrial cosmogenic nuclides (TCNs) to estimate burial ages of quartz-bearing sediments preserved in caves in the walls of the

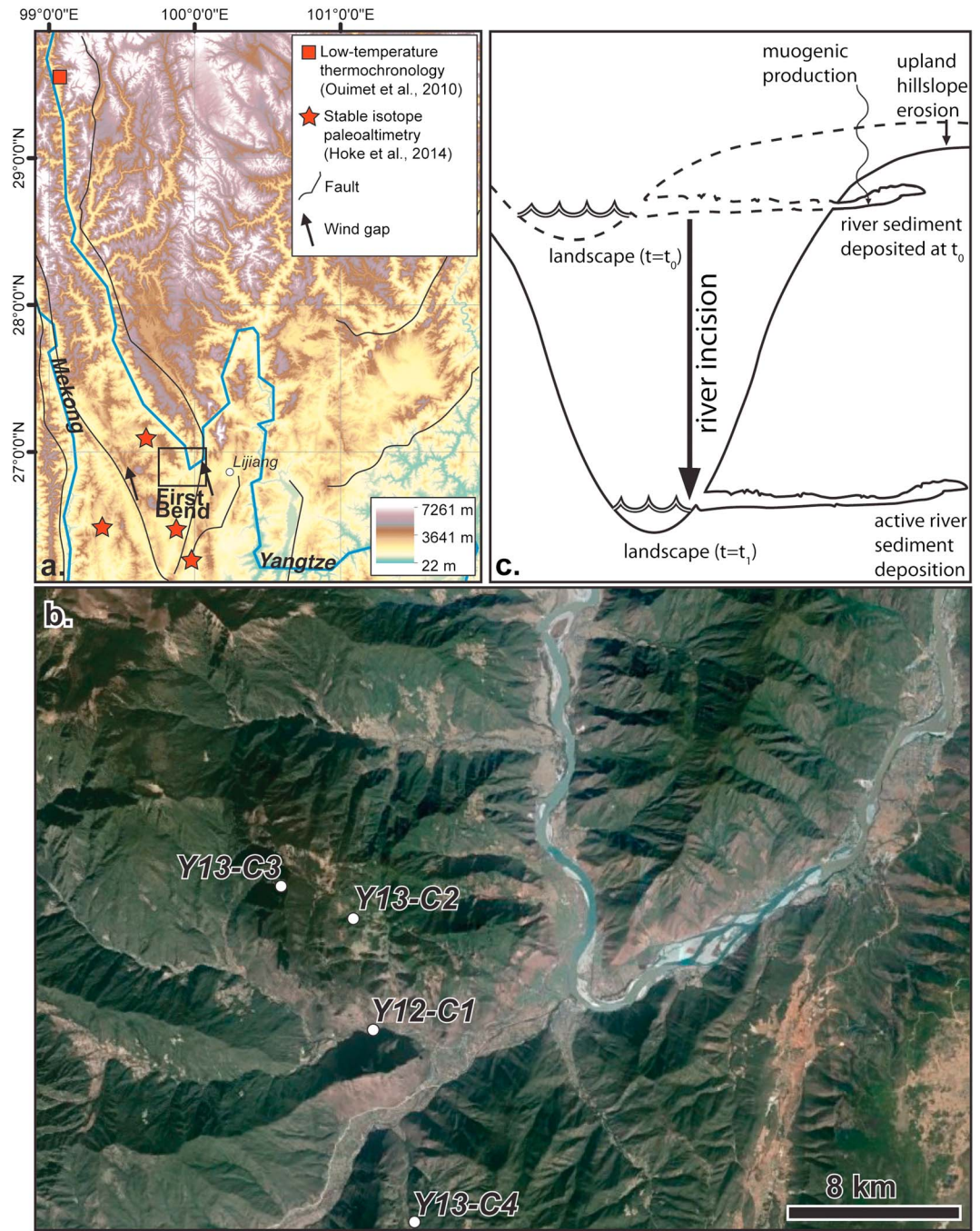


Figure 1. (a) Topographic map depicting the Yangtze River at the southeast margin of the Tibetan Plateau. Locations of relevant data are shown. (b) Positions of caves with fluvial quartz-bearing sediments. Map extent framed in Figure 1a. (c) Illustration of cave formation at the water table. As the river incises, lowering the water table, caves are abandoned on the walls of the gorge. Erosion removes sufficient overburden for in situ muogenic production of TCNs.

gorge [Granger *et al.*, 1997]. These sediments were deposited when the caves were near the level of the river and coarse bed load sediment was washed inside and buried. The river channel subsequently incised, abandoning the caves. We measured three TCNs (^{26}Al , ^{10}Be , and ^{21}Ne) for burial dating because we expected that incision occurred ~ 10 Ma or earlier on the basis of previous work [Clark *et al.*, 2005b; Ouimet *et al.*, 2010] and because the more common ^{26}Al — ^{10}Be technique cannot resolve burial ages older than ~ 8 Ma [Balco and Shuster, 2009a]. We further refine the three-nuclide burial age model in order to account for in situ muogenic

nuclide production. Our model explains both the absolute nuclide concentrations and their ratios and provides the capability to resolve burial ages >20 Ma. Finally, we report inverse model results from previously published thermochronologic data [Ouimet *et al.*, 2010], derived from sample sites located ~ 350 km upstream, and show that these results support our burial age calculations from the First Bend. Our work provides important new constraints on the timing of river capture as well as the rate of river incision since the middle Miocene.

2. Background

The bedrock at the First Bend is dominantly carbonate [Lacassin *et al.*, 1996] and caves exist throughout the landscape. Most often, the caves have shallow gradients and rounded cross sections that indicate formation as phreatic passages near the water table [Palmer, 1991]. When cave openings are exposed to the river, coarse bed load sediment may be washed inside, but caves are abandoned on the walls of the gorge as the river incises (Figure 1c). The burial ages of sediments from a series of caves therefore define the rate of river incision [Granger *et al.*, 1997]. On interfluvies, sinking streams may transport fine-grained sediment into abandoned caves from above, but they are unlikely to transport coarse bed load. This is particularly true around the First Bend, where there is no source of coarse, rounded quartz on the interfluvies above the caves. The most accessible caves are located in tributary gorges within a few kilometers of the Yangtze River. Their association with the regional water table, as well as the fact that cave openings are often paired on opposite sides of tributary gorges, suggests that these caves formed in close association with the Yangtze River trunk.

Regionally, many studies have examined river incision and surface uplift on the eastern and southeastern margin of the Tibetan Plateau. The earliest documented episode of exhumation occurred ~ 30 to 20 Ma [Wang *et al.*, 2012; Tian *et al.*, 2014]. By 15 to 10 Ma, rapid exhumation is well documented in thermochronology from the eastern and southeastern margins [Arne *et al.*, 1997; Kirby *et al.*, 2002; Clark *et al.*, 2005b; Godard *et al.*, 2009; Ouimet *et al.*, 2010; Wang *et al.*, 2012; Tian *et al.*, 2014]. This phase of exhumation has been interpreted to reflect river incision linked to the onset of surface uplift and crustal thickening via lower crustal flow [Clark *et al.*, 2005a, 2005b; Bai *et al.*, 2010; Ouimet *et al.*, 2010; Wang *et al.*, 2012]. However, this interpretation is inconsistent with the stable isotopic data, which suggest that the elevation of the region around the First Bend has remained near its present position since ~ 35 Ma [Hoke *et al.*, 2014; Li *et al.*, 2015]. If the stable isotope results are correct, then river incision is not a useful proxy for the timing of surface uplift. Surface uplift south of the plateau margin has progressed since ~ 13 Ma [Schoenbohm *et al.*, 2006; Hoke *et al.*, 2014; Li *et al.*, 2015].

3. Field and Laboratory Methods

In the field, we explored ~ 20 caves. We identified fluvial sediments in three caves perched above the modern river. These sediments consist of bedded sands and gravels with travertine caps. The beds often exhibit fluvial features such as ripples and scours (supporting information). In all cases, the fluvial deposits were located within 20 m of the cave openings, although we searched deeper. There was >10 m of bedrock shielding above sample Y13-C2, ~ 5 to 10 m above Y13-C3, and ≥ 10 m above Y13-C4. We sampled well-rounded quartz pebbles from each cave. We also sampled coarse sand from an active stream channel in a cave graded to the river along the present water table (Y12-C1). In the lab, we purified quartz and extracted ^{10}Be and ^{26}Al from samples using methods described in Corbett *et al.* [2013]. Accelerator mass spectrometer (AMS) measurements of ^{26}Al were made at Scottish Universities Environmental Research Centre [Xu *et al.*, 2015]. AMS measurements of ^{10}Be were made at Lawrence Livermore National Laboratory [Rood *et al.*, 2010]. Measurements of ^{21}Ne were made at the German Research Center for Geosciences using methods described in Niedermann *et al.* [1997] and Niedermann [2002]. See supporting information.

4. Burial Age Modeling

Conventional cosmogenic burial dating methods assume that nuclide production ceases at the time of sediment burial [Granger and Muzikar, 2001]. The main producers of TCNs at the surface—fast neutrons—attenuate rapidly with depth, such that production rates attributed to neutron spallation decrease by

a factor of 10^6 at a bedrock depth of ~ 8.5 m [Gosse and Phillips, 2001]. As a result, TCN concentrations measured in sediments sampled from beneath many tens of meters of overburden reflect the inheritance from past production on upstream hillslopes attenuated by decay since burial. Because TCNs are produced at proportional rates, the inherited ratios of surface-exposed material are initially constants. Following burial, radionuclide decay begins to alter the TCN ratios. The $^{26}\text{Al}/^{10}\text{Be}$ ratio at the time of production is ~ 6.85 for samples with a simple history of erosion and transport [Balco et al., 2008; Goethals et al., 2009]. Over time, the ratio declines in buried sediments. The $^{21}\text{Ne}/^{10}\text{Be}$ production rate ratio is ~ 4.08 and the nuclide ratio increases during burial because ^{21}Ne is stable [Balco and Shuster, 2009b; Goethals et al., 2009]. Using the concentrations of two nuclides and the assumption of a single exposure followed by burial, it is possible to solve for burial age and the initial nuclide concentrations at the time of burial. In addition, stable ^{21}Ne concentrations may be used independently to estimate initial radionuclide concentrations [Balco and Shuster, 2009a].

TCN production by muons after deposition violates an assumption underpinning the conventional burial age model. Muons account for a small fraction of total TCN production at the surface of the Earth, but the attenuation lengths associated with muogenic production pathways are 10 to 30 times greater than those associated with neutron spallation [e.g., Heisinger et al., 2002a, 2002b; Braucher et al., 2013]. As a result, muons can produce detectable concentrations of TCNs at depths of tens of meters. For radionuclides such as ^{26}Al and ^{10}Be , ratios (and concentrations) will eventually reflect in situ muogenic production, rather than the progressive decay away from the values inherited at the time of burial. Notably, however, in situ muogenic ^{21}Ne is insignificant compared to inherited ^{21}Ne because muogenic production rates are so low that muons are unlikely to account for more than a few percent of the inherited ^{21}Ne concentration, even after millions of years of burial [Goethals et al., 2009; Balco and Shuster, 2009b]. Consequently, the ^{26}Al — ^{10}Be — ^{21}Ne system may be used to detect violations of the assumption that TCN production stops upon burial. The key observations for in situ muogenic production are low radionuclide concentrations consistent with prolonged radionuclide decay, high $^{26}\text{Al}/^{10}\text{Be}$ ratios consistent with in situ production, and high $^{21}\text{Ne}/^{10}\text{Be}$ ratios consistent with prolonged ^{10}Be decay.

Because our samples at the First Bend were collected near cave entrances, where the topographic slopes limit the overburden thicknesses, we develop a burial age model that accounts for muogenic production (Figure 1c). The model assumes that sediment was washed into the caves near river level with initial TCN concentrations reflecting a simple history of exposure; this is consistent with the steep landscape and little opportunity for extended burial and sediment storage. The incising river then abandoned the caves and ongoing upland erosion gradually removed overburden, steadily driving an increase in the rate of TCN production by muons.

We infer that production by neutron spallation was insignificant because our sample sites have overburden thicknesses of ~ 10 m. Furthermore, these thicknesses are minima because erosion has progressively removed overburden from above. In our model, it is possible that the initial thickness was large enough that muogenic production was effectively zero, initially. Equation (1) describes the concentration of a cosmogenic radionuclide, N , subject to these boundary conditions:

$$N = \left[\frac{P_f z_f}{z_f \lambda + \varepsilon} e^{\left(\frac{z_f \lambda + \varepsilon}{z_f} t - \frac{z'}{z_f} \right)} + \frac{P_n z_n}{z_n \lambda + \varepsilon} e^{\left(\frac{z_n \lambda + \varepsilon}{z_n} t - \frac{z'}{z_n} \right)} - \frac{P_f z_f}{z_f \lambda + \varepsilon} e^{\left(-\frac{\varepsilon}{z_f} \right)} - \frac{P_n z_n}{z_n \lambda + \varepsilon} e^{\left(-\frac{\varepsilon}{z_n} \right)} + B \right] e^{-\lambda t}, \quad (1)$$

where subscripts f and n refer to fast and captured negative muons, respectively; P , surface production rate; z , attenuation length; z' , overburden thickness at time of burial; λ , radionuclide decay constant; ε , rate of overburden erosion; t , burial age; and B , radionuclide concentration at the time of burial. Values for P may be estimated from the literature (supporting information). We must constrain the remaining parameters to solve for burial age. We determine initial radionuclide concentrations and erosion rate using ^{21}Ne . The ^{21}Ne concentration in a now buried sample reflects production on upland hillslopes, meaning that we can calculate drainage-average hillslope erosion rate from ^{21}Ne using standard methods [e.g., Bierman and Steig, 1996] (supporting information). This rate is not the same as the rate of gorge incision. We then assume that this erosion rate is similar to the subsequent rate of overburden erosion directly above the sample. Finally, we write two versions of equation (1) (for ^{26}Al and ^{10}Be , respectively) and solve simultaneously for initial overburden thickness and burial age.

Table 1. Results

Elevation (m) ^a	Sample ID ^b	¹⁰ Be (×10 ⁴ atoms/g) ^c	²⁶ Al (×10 ⁴ atoms/g) ^d	²¹ Ne (×10 ⁶ atoms/g) ^e	²⁶ Al/ ¹⁰ Be ^f	²¹ Ne/ ¹⁰ Be ^f	²¹ Ne-Derived Burial Age (Ma) ^g	Radionuclide-Derived Burial Age (Ma) ^h
1875	Y12-C1	34.1 ± 1.5	212.0 ± 9.5	2.1 (+1.2/−1.0)	6.2 ± 0.4	6.2 (+3.5/−2.9)	-	-
2285	Y13-C4	1.97 ± 0.13	15.4 ± 2.6	3.8 (+1.5/−1.0)	6.6 ± 1.1	189 (+76/−51)	15.4 (+14.4/−3.5)	9.2 (+0.6/−0.6)
2285	Y13-C4x	2.07 ± 0.14	12.1 ± 1.3	-	-	-	-	-
2905	Y13-C2	1.04 ± 0.10	6.6 ± 1.1	2.49 (+0.93/−0.75)	6.3 ± 1.2	241 (+93/−76)	12.8 (+5.3/−0.8)	10.5 (+0.5/−0.4)
3320	Y13-C3	0.905 ± 0.097	6.5 ± 1.1	7.8 (+1.0/−0.7)	7.1 ± 1.4	850 (+140/−120)	36.6 (+0.6/−2.8)	12.4 (+1.3/−1.1)
3320	Y13-C3x	0.93 ± 0.10	-	-	-	-	-	-

^aRiver is at 1860 m. See text and supporting information for details on setting within caves.

^bAn “x” indicates a replicate split following quartz purification.

^cBlank-corrected values measured at Lawrence Livermore National Laboratory using 07KNSTD. Uncertainty at 2 s. See supporting information.

^dBlank-corrected values measured at SUERC using Z92-0222. Uncertainty at 2 s. See supporting information.

^eMeasured at GFZ. Uncertainty at 2 s. See supporting information.

^fUncertainty-weighted average where replicates are available.

^gCalculated using ²¹Ne to infer initial radionuclide concentrations. Uncertainty at 68% confidence level. See text.

^hCalculated using radionuclide data from Y12-C1 for initial radionuclide concentrations. Uncertainty at 68% confidence level. See text.

We can also calculate an alternative set of burial ages without using ²¹Ne. Instead, we estimate the rate of overburden erosion and the initial radionuclide concentrations from the sample we collected in a fluvially active cave at river level (Y12-C1). If we assume that the radionuclide concentrations in river sediments have remained constant through time, then we can use the river level sample directly as an estimator of initial radionuclide concentrations in other cave samples (note that the burial age of mobile cave sediment is insignificant). This is a restrictive assumption, but it provides an alternative estimate of initial concentration that is independent of ²¹Ne, which has large analytical uncertainties. We then calculate drainage-average erosion rates using these values and solve simultaneously for initial overburden thickness and burial age.

Muogenic production rates described by *Heisinger et al.* [2002a, 2002b] are thought to be too high [*Balco et al.*, 2008; *Braucher et al.*, 2011, 2013]. Therefore, we report burial ages using muogenic production rates calculated from the muon interaction cross sections described in *Balco et al.* [2013]. Burial ages calculated from the earlier cross sections are systematically older by an average of 29%, but this offset does not alter our conclusions (supporting information).

5. Thermochronologic Modeling

We support our burial age and incision rate calculations using a vertical transect of low-temperature thermochronology from ~350 km upstream of the First Bend, reported by *Ouimet et al.* [2010] (Figure 1). This is the nearest transect available with the low-elevation samples necessary to resolve recent incision. The distance from the First Bend is relatively unimportant because the entire longitudinal profile of the river will typically adjust to external forcing by tectonic surface uplift or climate change. In order to constrain cooling rates, we model the reproducible apatite and zircon (U-Th)/He data from this vertical transect using Qtqt [*Gallagher*, 2012]. We interpret the cooling rates to reflect exhumation by river incision at the point of sampling. This approach is more complete than the interpretation presented in *Ouimet et al.* [2010] because it accounts for the geologically recent erosion necessary to bring the samples to the surface. We are therefore better able to resolve post-7 Ma cooling, which *Ouimet et al.* [2010] did not consider in detail.

6. Results

Together, cosmogenic ²⁶Al, ¹⁰Be, and ²¹Ne concentrations can be used to reconstruct both paleoerosion rates and the history of river incision. ²¹Ne concentrations are indistinguishable within error among samples from the two lower elevation abandoned caves as well as the fluvially active cave at the present river level (Table 1), implying a steady upstream hillslope erosion rate of 21 ± 9 mm/kyr since ~13 Ma. This erosion rate is consistent with detrital ¹⁰Be estimates of 13 to 42 mm/kyr from the modern Yangtze River [*Henck et al.*, 2011]. The sample from the highest elevation abandoned cave has a substantially higher ²¹Ne concentration, implying a lower drainage-average erosion rate (7.5 ± 1.0 mm/kyr) in the more distant past.

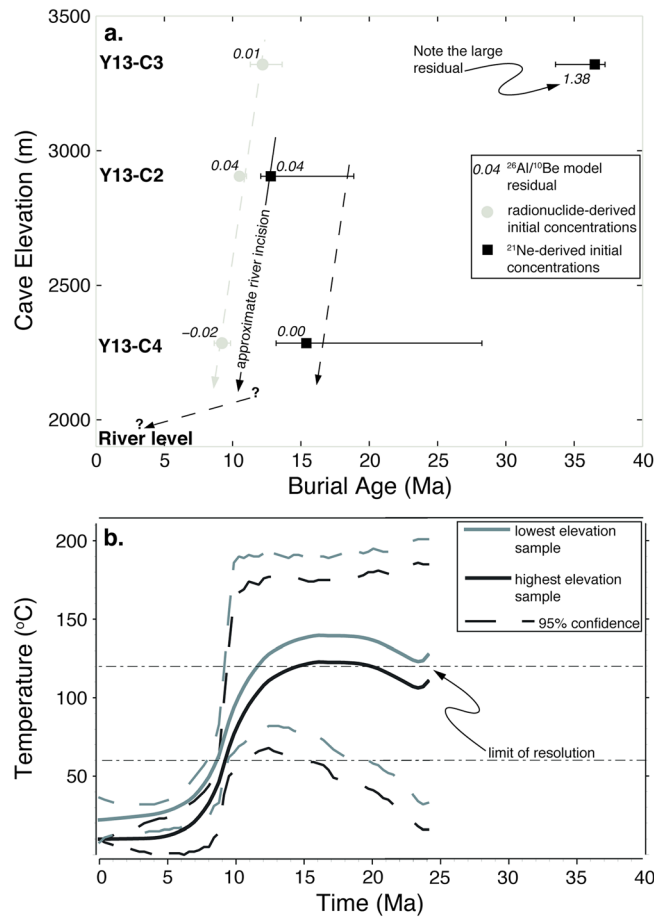


Figure 2. (a) Burial ages plotted against cave elevation. Error bars reflect bootstrapped confidence intervals (68%). Residual $^{26}\text{Al}/^{10}\text{Be}$ ratios are observed minus predicted. (b) Best estimate time-temperature paths for the highest and lowest elevation thermochronology samples (Figure 1a).

consider the oldest ^{21}Ne -derived age an outlier because its residual is 35 times larger than any other (Figure 2a). Calculated using the river level (Y12-C1) data for initial ^{26}Al and ^{10}Be concentrations, the burial ages are 9.2, 11, and 12 Ma. We report 68% confidence intervals for these burial ages, which are estimated using a bootstrap approach with 1000 replicates per sample (Table 1). As discussed below, other important sources of uncertainty are difficult to quantify.

The most probable time-temperature paths inverted from thermochronology upstream of the First Bend are consistent with our burial age results (Figure 2b). One-dimensional modeling favors a phase of rapid cooling, presumably via river incision, beginning at ~ 12 Ma, followed by much slower cooling since ~ 7 Ma.

7. Model Assessment

Compared to conventional ^{26}Al — ^{10}Be burial dating [Granger and Muzikar, 2001], our approach is advantageous because it allows for the measurement of burial ages older than ~ 8 Ma. ^{26}Al — ^{10}Be calculations, without accounting for in situ muogenic production, yield burial ages of < 0.25 Ma at the First Bend, clearly in error. Such young ages imply an incision rate approaching 10 m/kyr, which is implausible in light of the other estimates of erosion and incision rates in the region, which are at least an order of magnitude lower [Clark et al., 2005b; Ouimet et al., 2009, 2010; Henck et al., 2011]. Alternatively, the young ^{26}Al — ^{10}Be burial ages might suggest recent sediment transport into the caves, but the difference in nuclide concentrations between the abandoned caves and the active cave would require dramatically different sediment sources in that case, which is unlikely given their close proximity (Figure 1).

In contrast, ^{26}Al and ^{10}Be concentrations in the sediment from abandoned caves are an order of magnitude lower than in the sediment from the active cave (Table 1), consistent with extended burial and radio decay. The $^{26}\text{Al}/^{10}\text{Be}$ ratios in both the abandoned caves and the active cave are > 6.2 and indistinguishable within error. Drainage-average erosion rates calculated from the ^{26}Al and ^{10}Be concentrations in the active cave sediment sample (Y12-C1) are 45.3 ± 2.0 mm/kyr and 42.0 ± 1.9 mm/kyr, respectively, which are consistent with the estimate from the ^{21}Ne concentration in the same sample (28 ± 16 mm/kyr). The $^{21}\text{Ne}/^{10}\text{Be}$ ratios of abandoned cave samples are 2 to 3 orders of magnitude larger than the production rate ratio [Balco and Shuster, 2009b], implying significant decay of ^{10}Be and thus very long burial ages.

In situ muogenic production simultaneously explains the low radionuclide concentrations, high $^{26}\text{Al}/^{10}\text{Be}$ ratios, and high $^{21}\text{Ne}/^{10}\text{Be}$ ratios. When the initial concentrations of ^{26}Al and ^{10}Be are estimated from ^{21}Ne concentrations in the respective samples, the burial ages of the abandoned caves are 15, 13, and 37 Ma in order from lowest elevation to highest (Figure 2a). We con-

Burial ages, calculated using initial concentrations derived from either ^{21}Ne or radionuclides, both indicate that the incision rate declined substantially following a period of rapid Miocene downcutting. The timing of this decline is less certain. Viewing the calculations separately, rapid incision was occurring between either 18 and 12 Ma or 13 and 9 Ma, depending on the choice of initial concentrations and allowing for analytical uncertainties (Figure 2a). However, we favor interpreting both burial age calculations at each cave as if they were replicates. This approach emphasizes that different burial age calculations involve different assumptions, and comparison of different calculations constrains the validity of those assumptions. Viewed in this manner, and subject to age superposition, the river likely incised >0.6 km from the level of Y13-C2 to Y13-C4 between ~ 13 and 11 Ma. We have fewer constraints on the 0.4 km of incision between Y13-C3 and Y13-C2 because we exclude the ^{21}Ne result at Y13-C3 as an outlier.

Perhaps the most difficult uncertainty to quantify is our assumption that drainage-average erosion rates have remained constant, which is required for burial ages calculated with radionuclide-derived initial concentrations. ^{21}Ne results from the active, river level cave (Y12-C1) provide useful information. The ^{21}Ne concentration from Y12-C1 is indistinguishable from the concentrations in the two higher, abandoned caves (Y13-C4 and Y13-C2). This implies that drainage-average erosion rates were also similar. The large upstream drainage area, including abundant low-relief landscapes, may explain how the drainage-average erosion rate was buffered despite the incision of a deep gorge. The ^{21}Ne concentration at the highest elevation cave (Y13-C3) is more than twice the other values. This may reflect a more complex history of exposure and burial than our model accounts for—an interpretation supported by the large $^{26}\text{Al}/^{10}\text{Be}$ residual (Figure 2a). In light of results from lower elevation caves, we tentatively accept the burial age calculated at Y13-C3 using radionuclide-derived initial concentrations, recognizing that this age is subject to uncertainties at least as great as the differences between replicates at lower elevations ($\sim 50\%$).

Finally, thermochronology provides an additional, independent constraint on river incision, which also supports our burial age interpretation: rapid incision in the Miocene, followed by a decline in rate after that time (Figure 2b).

8. Implications

Our results indicate that the gorge at the First Bend achieved most of its depth between 18 and 9 Ma (Figure 2). In particular, the channel incised at that time below the elevation of the Yangpai Gap and its eastward extension (~ 2400 and 3300 m, respectively), described by *Clark et al.* [2004], and the wind gap near Luoguqing (~ 3400 m), described by *Kong et al.* [2012]. These wind gaps describe the hypothesized courses of an ancient, south-flowing river prior to capture by the modern Yangtze. Incision below the elevations of the gaps suggests that capture occurred prior to 9 Ma at the First Bend. Therefore, if river capture occurred, it was likely prior to middle Miocene, as proposed by *Clift* [2006].

Notably, we demonstrate a marked decline in the rate of river incision near the end of the Miocene (Figure 2). Local fault activity may explain the decline, in part. Just downstream from the First Bend, the active normal fault located at Tiger Leaping Gorge has a reported slip rate of 5 m/kyr [*Kong et al.*, 2010; *Van der Woerd et al.*, 2012]. Surface uplift as a result of flexural bending in the footwall of this east-dipping structure could reduce the stream gradient in the vicinity of the First Bend, locally ending incision and driving aggradation [e.g., *Wang et al.*, 2014]. Recent drilling near the First Bend shows that as much as 300 m of sediment has aggraded in parts of the valley since sometime before ~ 2 Ma [*Zhao et al.*, 2015]. The position of the fault corresponds with a major knickpoint, which has set the local base level and has potentially led to an upstream decline in incision rate [*Liu-Zeng et al.*, 2008]. However, the close temporal coincidence of the decline of stream incision at the First Bend and at the thermochronology transect ~ 350 km upstream [*Ouimet et al.*, 2010] suggests another, regionally extensive process also contributed to the decline of incision rates.

In southeastern Tibet, major rivers are often assumed to maintain a quasi-steady state, that is, the rivers respond rapidly to changing boundary conditions such that incision balances surface uplift [e.g., *Clark et al.*, 2005b, 2006]. If the Yangtze River near the First Bend has maintained a quasi-steady state profile, then the post-late Miocene decline in incision rate implies that the rate of tectonic surface uplift also declined at around that time. Recent modeling suggests a mechanism for declining uplift [*Cook and Royden*, 2008]. In this model, the growing Tibetan Plateau rapidly expands when it encounters a zone of weak lower crust on the

southeast margin. The topographic surface experiences rapid surface uplift followed by a declining uplift rate as the plateau margin approaches the elevation of the plateau itself. However, this model scenario does not apply to the First Bend because the First Bend has not yet approached the elevation of the plateau at >4 km—it is located immediately below a steep topographic shelf at an elevation of <3 km [Liu-Zeng *et al.*, 2008]. As a result, declining river incision rates are difficult to explain simply as a response to lower crustal flow.

Alternatively, river networks may remain far from equilibrium for long periods and suddenly readjust with a transient pulse of incision when climate, sediment load, or other conditions become favorable [Sklar and Dietrich, 2004; Pelletier, 2007]. Dramatically nonsteady state behavior has been documented on the Yellow River in northeastern Tibet [Craddock *et al.*, 2010]. On the southeast margin, the contrast between stable isotope results—which indicate that the First Bend has been near its present elevation since the Eocene [Hoke *et al.*, 2014; Li *et al.*, 2015]—and thermochronologic results—which indicate river incision in the major upstream tributaries began ~13 Ma [Clark *et al.*, 2005b; Ouimet *et al.*, 2010]—suggests a considerable lag between uplift and incision. In this case, the decline in incision rates may simply reflect the conclusion of a transient adjustment. Although river incision is not a valid constraint on the timing of surface uplift in this unsteady scenario, our results implicitly support the stable isotope paleoaltimetry, indicating that little surface uplift has occurred on the southeast margin since the Eocene.

9. Conclusions

TCN burial ages derived from abandoned cave sediments indicate that the Yangtze River incised most of the gorge at the First Bend between 18 and 9 Ma. River incision slowed substantially thereafter. We are able to resolve middle Miocene burial ages by using a model that accounts for in situ muogenic production in buried cave sediments. This model provides an internally consistent explanation for the concentrations of ^{10}Be , ^{26}Al , and ^{21}Ne , as well as the $^{26}\text{Al}/^{10}\text{Be}$ and $^{21}\text{Ne}/^{10}\text{Be}$ ratios. Low-temperature thermochronology from ~350 km upstream of the First Bend supports both rapid incision and subsequent slowing of incision.

The timing of incision at the First Bend has important implications for the geodynamic history of the southeast margin of the Tibetan Plateau. First, the fact that the gorge incised below hypothesized wind gaps by 9 Ma strongly supports an early capture event for the integration of the upper Yangtze River. Second, the decline of river incision rate around the late Miocene is inconsistent with current models of surface uplift driven by lower crustal flow. Although this inconsistency does not preclude lower crustal flow, it challenges existing models and highlights the difficulty of using the timing of river incision as a proxy for the timing of surface uplift.

Acknowledgments

This work was supported by NSF award EAR 1019427 to G.D.H. and NSFC award 41172179 to J.L.-Z. The authors thank Yan Li and Zhiming Fung for field support and Enzo Schnabel for noble gas analyses. Amanda Schmidt and an anonymous reviewer provided constructive criticisms.

References

- Arne, D., B. Worley, C. Wilson, S. F. Chen, D. Foster, Z. L. Luo, S. G. Liu, and P. Dirks (1997), Differential exhumation in response to episodic thrusting along the eastern margin of the Tibetan Plateau, *Tectonophysics*, *280*, 239–256.
- Bai, D., *et al.* (2010), Crustal deformation of the eastern Tibetan Plateau revealed by magnetotelluric imaging, *Nat. Geosci.*, *3*(5), 358–362, doi:10.1038/ngeo830.
- Balco, G., and D. L. Shuster (2009a), ^{26}Al - ^{10}Be - ^{21}Ne burial dating, *Earth Planet. Sci. Lett.*, *286*(3–4), 570–575, doi:10.1016/j.epsl.2009.07.025.
- Balco, G., and D. L. Shuster (2009b), Production rate of cosmogenic ^{21}Ne in quartz estimated from ^{10}Be , ^{26}Al , and ^{21}Ne concentrations in slowly eroding Antarctic bedrock surfaces, *Earth Planet. Sci. Lett.*, *281*(1–2), 48–58, doi:10.1016/j.epsl.2009.02.006.
- Balco, G., J. O. Stone, N. A. Lifton, and T. J. Dunai (2008), A complete and easily accessible means of calculating surface exposure ages or erosion rates from ^{10}Be and ^{26}Al measurements, *Quat. Geochronol.*, *3*(3), 174–195, doi:10.1016/j.quageo.2007.12.001.
- Balco, G., G. S. Soreghan, D. E. Sweet, K. R. Marra, and P. R. Bierman (2013), Cosmogenic-nuclide burial ages for Pleistocene sedimentary fill in Unaweep Canyon, Colorado, USA, *Quat. Geochronol.*, *18*(C), 149–157, doi:10.1016/j.quageo.2013.02.002.
- Barbour, G. B. (1936), Physiographic history of the Yangtze, *Geogr. J.*, *87*(1), 17–32, doi:10.2307/1786198.
- Bierman, P., and E. J. Steig (1996), Estimating rates of denudation using cosmogenic isotope abundances in sediment, *Earth Surf. Process. Landforms*, *21*, 125–139.
- Braucher, R., S. Merchel, J. Borgomano, and D. L. Bourlès (2011), Production of cosmogenic radionuclides at great depth: A multi element approach, *Earth Planet. Sci. Lett.*, *309*(1–2), 1–9, doi:10.1016/j.epsl.2011.06.036.
- Braucher, R., *et al.* (2013), Determination of muon attenuation lengths in depth profiles from in situ produced cosmogenic nuclides, *Nuclear Instrum. Methods Phys. Res. B*, *294*(C), 484–490, doi:10.1016/j.nimb.2012.05.023.
- Clark, M. K., and L. H. Royden (2000), Topographic ooze: Building the eastern margin of Tibet by lower crustal flow, *Geology*, *28*(8), 703–706.
- Clark, M. K., L. M. Schoenbohm, L. H. Royden, K. X. Whipple, B. C. Burchfiel, X. Zhang, W. Tang, E. Wang, and L. Chen (2004), Surface uplift, tectonics, and erosion of eastern Tibet from large-scale drainage patterns, *Tectonics*, *23*, TC1006, doi:10.1029/2002TC001402.
- Clark, M. K., J. W. M. Bush, and L. H. Royden (2005a), Dynamic topography produced by lower crustal flow against rheological strength heterogeneities bordering the Tibetan Plateau, *Geophys. J. Int.*, *162*(2), 575–590, doi:10.1111/j.1365-246X.2005.02580.x.
- Clark, M. K., M. A. House, L. H. Royden, K. X. Whipple, B. C. Burchfiel, X. Zhang, and W. Tang (2005b), Late Cenozoic uplift of southeastern Tibet, *Geology*, *33*(6), 525–528, doi:10.1130/G21265.1.

- Clark, M. K., L. H. Royden, K. X. Whipple, B. C. Burchfiel, X. Zhang, and W. Tang (2006), Use of a regional, relict landscape to measure vertical deformation of the eastern Tibetan Plateau, *J. Geophys. Res.*, *111*, F03002, doi:10.1029/2005JF000294.
- Clift, P. D. (2006), Controls on the erosion of Cenozoic Asia and the flux of clastic sediment to the ocean, *Earth Planet. Sci. Lett.*, *241*(3–4), 571–580, doi:10.1016/j.epsl.2005.11.028.
- Cook, K. L., and L. H. Royden (2008), The role of crustal strength variations in shaping orogenic plateaus, with application to Tibet, *J. Geophys. Res.*, *113*, B08407, doi:10.1029/2007JB005457.
- Corbett, L. B., P. R. Bierman, J. A. Graly, T. A. Neumann, and D. H. Rood (2013), Constraining landscape history and glacial erosivity using paired cosmogenic nuclides in Upernavik, northwest Greenland, *Geol. Soc. Am. Bull.*, *125*(9–10), 1539–1553, doi:10.1130/B30813.1.
- Craddock, W. H., E. Kirby, N. W. Harkins, H. Zhang, X. Shi, and J. Liu (2010), Rapid fluvial incision along the Yellow River during headward basin integration, *Nat. Geosci.*, *3*(3), 209–213, doi:10.1038/ngeo777.
- Gallagher, K. (2012), Transdimensional inverse thermal history modeling for quantitative thermochronology, *J. Geophys. Res.*, *117*, B02408, doi:10.1029/2011JB008825.
- Godard, V., J. Lavé, J. Carcaillet, R. Cattin, D. Bourlès, and J. Zhu (2009), Spatial distribution of denudation in Eastern Tibet and regressive erosion of plateau margins, *Tectonophysics*, *491*(1), 1–22, doi:10.1016/j.tecto.2009.10.026.
- Goethals, M. M., R. Hetzel, S. Niedermann, H. Wittmann, C. R. Fenton, P. W. Kubik, M. Christl, and F. von Blanckenburg (2009), An improved experimental determination of cosmogenic $^{10}\text{Be}/^{21}\text{Ne}$ and $^{26}\text{Al}/^{21}\text{Ne}$ production ratios in quartz, *Earth Planet. Sci. Lett.*, *284*(1–2), 187–198, doi:10.1016/j.epsl.2009.04.027.
- Gosse, J. C., and F. M. Phillips (2001), Terrestrial in situ cosmogenic nuclides: Theory and application, *Quat. Sci. Rev.*, *20*(14), 1475–1560, doi:10.1016/S0277-3791(00)00171-2.
- Granger, D. E., and P. Muzikar (2001), Dating sediment burial with in situ-produced cosmogenic nuclides: Theory, techniques, and limitations, *Earth Planet. Sci. Lett.*, *118*, 269–281.
- Granger, D. E., J. W. Kirchner, and R. C. Finkel (1997), Quaternary downcutting rate of the New River, Virginia, measured from differential decay of cosmogenic ^{26}Al and ^{10}Be in cave-deposited alluvium, *Geology*, *25*, 107–110.
- Heisinger, B., D. Lal, A. J. T. Jull, P. Kubik, S. Ivy-Ochs, S. Neumaier, K. Knie, V. Lazarev, and E. Nolte (2002a), Production of selected cosmogenic radionuclides by muons: 1. Fast muons, *Earth Planet. Sci. Lett.*, *200*(3–4), 345–355, doi:10.1016/S0012-821X(02)00640-4.
- Heisinger, B., D. Lal, A. J. T. Jull, P. Kubik, S. Ivy-Ochs, K. Knie, and E. Nolte (2002b), Production of selected cosmogenic radionuclides by muons: 2. Capture of negative muons, *Earth Planet. Sci. Lett.*, *200*(3–4), 357–369, doi:10.1016/S0012-821X(02)00641-6.
- Henck, A. C., K. W. Huntington, J. O. Stone, D. R. Montgomery, and B. Hallet (2011), Spatial controls on erosion in the Three Rivers Region, southeastern Tibet and southwestern China, *Earth Planet. Sci. Lett.*, *303*(1–2), 71–83, doi:10.1016/j.epsl.2010.12.038.
- Herman, F., D. Seward, P. G. Valla, A. Carter, B. Kohn, S. D. Willett, and T. A. Ehlers (2014), Worldwide acceleration of mountain erosion under a cooling climate, *Nature*, *504*(7480), 423–426, doi:10.1038/nature12877.
- Hoke, G. D., J. Liu-Zeng, M. T. Hren, C. N. Garzzone, and G. K. Wissink (2014), Stable isotopes reveal high southeast Tibetan Plateau margin since the Paleogene, *Earth Planet. Sci. Lett.*, *394*(C), 270–278, doi:10.1016/j.epsl.2014.03.007.
- Kirby, E., P. W. Reiners, M. A. Krol, K. X. Whipple, K. V. Hodges, K. A. Farley, W. Tang, and Z. Chen (2002), Late Cenozoic evolution of the eastern margin of the Tibetan Plateau: Inferences from $^{40}\text{Ar}/^{39}\text{Ar}$ and (U-Th)/He thermochronology, *Tectonics*, *21*(1), 1001, doi:10.1029/2000TC001246.
- Kong, P., D. E. Granger, F. Wu, M. W. Caffee, Y. J. Wang, Z. Xi-Tao, and Y. Zheng (2009), Cosmogenic nuclide burial ages and provenance of the Xigeda paleo-lake: Implications for evolution of the Middle Yangtze River, *Earth Planet. Sci. Lett.*, *278*(1–2), 131–141, doi:10.1016/j.epsl.2008.12.003.
- Kong, P., D. Fink, C. Na, and W. Xiao (2010), Dip-slip rate determined by cosmogenic surface dating on a Holocene scarp of the Daju fault, Yunnan, China, *Tectonophysics*, *493*, 106–112.
- Kong, P., Y. Zheng, and M. W. Caffee (2012), Provenance and time constraints on the formation of the first bend of the Yangtze River, *Geochem. Geophys. Geosyst.*, *13*, Q06017, doi:10.1029/2012GC004140.
- Lacassin, R., U. Schärer, P. H. Leloup, N. Arnaud, P. Tapponnier, X. Liu, and L. Zhang (1996), Tertiary deformation and metamorphism SE of Tibet: The folded Tiger-leap décollement of NW Yunnan, China, *Tectonics*, *15*(3), 605–622, doi:10.1029/95TC03749.
- Lee, C. Y. (1934), The development of the upper Yangtze Valley, *Bull. Geol. Soc. China*, *13*(1), 107–118, doi:10.1111/j.1755-6724.1934.mp13001006.x.
- Li, S., B. S. Currie, D. B. Rowley, and M. Ingalls (2015), Cenozoic paleoaltimetry of the SE margin of the Tibetan Plateau: Constraints on the tectonic evolution of the region, *Earth Planet. Sci. Lett.*, *432*, 415–424.
- Liu-Zeng, J., P. Tapponnier, Y. Gaudemer, and L. Ding (2008), Quantifying landscape differences across the Tibetan plateau: Implications for topographic relief evolution, *J. Geophys. Res.*, *113*, F04018, doi:10.1029/2007JF000897.
- Niedermann, S. (2002), Cosmic-ray-produced noble gases in terrestrial rocks: Dating tools for surface processes, *Rev. Mineral. Geochem.*, *47*, 731–784.
- Niedermann, S., W. Bach, and J. Erzinger (1997), Noble gas evidence for a lower mantle component in MORBs from the southern East Pacific Rise: Decoupling of helium and neon isotope systematics, *Geochim. Cosmochim. Acta*, *61*, 2697–2715.
- Quimet, W. B., K. X. Whipple, and D. E. Granger (2009), Beyond threshold hillslopes: Channel adjustment to base-level fall in tectonically active mountain ranges, *Geology*, *37*(7), 579–582, doi:10.1130/G30013A.1.
- Quimet, W., K. X. Whipple, L. Royden, P. Reiners, K. Hodges, and M. Pringle (2010), Regional incision of the eastern margin of the Tibetan Plateau, *Lithosphere*, *2*(1), 50–63, doi:10.1130/L57.1.
- Palmer, A. N. (1991), Origin and morphology of limestone caves, *Geol. Soc. Am. Bull.*, *103*(1), 1–21.
- Pelletier, J. D. (2007), Numerical modeling of the Cenozoic geomorphic evolution of the southern Sierra Nevada, California, *Earth Planet. Sci. Lett.*, *259*(1–2), 85–96, doi:10.1016/j.epsl.2007.04.030.
- Rood, D. H., S. Hall, T. P. Guilderson, R. C. Finkel, and T. A. Brown (2010), Challenges and opportunities in high-precision Be-10 measurements at CAMS, *Nuclear Instrum. Methods Phys. Res. Section B: Beam Interactions with Mater. Atoms*, *268*(7–8), 730–732, doi:10.1016/j.nimb.2009.10.016.
- Royden, L. H., B. C. Burchfiel, R. W. King, E. Wang, Z. Chen, F. Shen, and Y. Liu (1997), Surface deformation and lower crustal flow in eastern Tibet, *Science*, *276*(5313), 788–790, doi:10.1126/science.276.5313.788.
- Royden, L. H., B. C. Burchfiel, and R. D. van der Hilst (2008), The geological evolution of the Tibetan Plateau, *Science*, *321*(5892), 1054–1058, doi:10.1126/science.1155371.
- Schoenbohm, L. M., B. C. Burchfiel, and C. Liangzhong (2006), Propagation of surface uplift, lower crustal flow, and Cenozoic tectonics of the southeast margin of the Tibetan Plateau, *Geology*, *34*(10), 813, doi:10.1130/G22679.1.
- Sklar, L. S., and W. E. Dietrich (2004), A mechanistic model for river incision into bedrock by saltating bed load, *Water Resour. Res.*, *40*, W06301, doi:10.1029/2003WR002496.

- Tapponnier, P. (2001), Oblique stepwise rise and growth of the Tibet Plateau, *Science*, *294*(5547), 1671–1677, doi:10.1126/science.105978.
- Tapponnier, P., J. L. Mercier, F. Proust, and J. Andrieux (1981), The Tibetan side of the India–Eurasia collision, *Nature*, *294*(5840), 405–410, doi:10.1038/294405a0.
- Tian, Y., B. P. Kohn, and A. Gleadow (2014), A thermochronological perspective on the morphotectonic evolution of the southeastern Tibetan Plateau, *J. Geophys. Res. Solid Earth*, *676*–698, doi:10.1002/2013JB010429.
- Van der Woerd, J., A. Perrineau, Y. Gaudemer, P. H. Leloup, L. Barrier, and R. Thuzet (2012), Extensional step-over between the Zhongdian and Red River faults: Kinematics of the Daju normal fault constrained by cosmogenic dating of the Yangtze terraces (Yulong Shan, Yunnan) European Geophysical Union General Assembly Conference Abstracts, 14, EGU General Assembly 2012, held 22–27 April, 2012 in Vienna, Austria., p. 10971.
- Wang, E., B. C. Burchfiel, L. H. Royden, L. Chen, J. Chen, W. Li, and C. Zhiliang (1998), Late Cenozoic Xianshuihe–Xiaojiang, Red River, and Dali fault systems of southwestern Sichuan and central Yunnan, China, *Geol. Soc. Am. Spec. Pap.*, *327*, 1–108.
- Wang, E., E. Kirby, K. P. Furlong, M. van Soest, G. Xu, X. Shi, P. J. J. Kamp, and K. V. Hodges (2012), Two-phase growth of high topography in eastern Tibet during the Cenozoic, *Nat. Geosci.*, *5*(9), 640–645, doi:10.1038/ngeo1538.
- Wang, P., D. Scherler, J. Liu-Zeng, J. Mey, J. P. Avouac, Y. Zhang, and D. Shi (2014), Tectonic control of Yarlung Tsangpo Gorge revealed by a buried canyon in Southern Tibet, *Science*, *346*(6212), 978–981, doi:10.1126/science.1259041.
- Xu, S., S. Freeman, D. H. Rood, and R. P. Shanks (2015), Decadal ^{10}Be , ^{26}Al and ^{36}Cl QA measurements on the SUERC 5MV accelerator mass spectrometer, *Nuclear Instrum. Methods Phys. Res. B*, *361*, 39–42, doi:10.1016/j.nimb.2015.03.064.
- Yan, Y., A. Carter, C.-Y. Huang, L.-S. Chan, X.-Q. Hu, and Q. Lan (2012), Constraints on Cenozoic regional drainage evolution of SW China from the provenance of the Jianchuan Basin, *Geochem. Geophys. Geosyst.*, *13*, Q11008, doi:10.1029/2011GC003803.
- Zhao, X., Z. Wu, Y. Feng, Y. Zhang, D. Hu, Y. Qu, and C. Guo (2015), Landscapes and sediments of the 'Yangtze First Bend valley' along the Jinsha river and the development of the valley, *Geol. Bull.China*, *34*, 1–21.